JOURNAL OF SPACECRAFT AND ROCKETS
Vol. 36, No. 3, May–June 1999

Direct Simulation Monte Carlo Calculations of Aerothermodynamics for Mars Microprobe Capsules

James N. Moss,* Richard G. Wilmoth,† and Joseph M. Price‡
NASA Langley Research Center, Hampton, Virginia 23681

The hypersonic transitional flow aerodynamics of the Mars Microprobe capsules are simulated with the direct simulation Monte Carlo method. Calculations of axial, normal, and static pitching coefficients were obtained over an angle-of-attack range comparable to actual flight requirements. Comparisons are made with modified Newtonian and free-molecular flow calculations. Aerothermal results were also obtained for zero incidence entry conditions. The current aerodynamic results are shown to be in excellent agreement with Navier–Stokes results for small Knudsen number conditions. Peak heating conditions occur under rarefied conditions where the heating becomes a strong function of assumptions concerning surface catalytic activity.

Nomenclature

C_A = axial force coefficient
C_D = drag coefficient
$C_{D,P}$ = drag coefficient due to pressure
C_i = mass fraction of species i
C_L = lift coefficient
$C_{m,\mathrm{cg}}$ = pitching-moment coefficient about center of gravity
$C_{m,0}$ = pitching-moment coefficient about nose
C_N = normal force coefficient
d = maximum probe diameter, m
Kn = Knudsen number
p = pressure, N/m^2
q = heat transfer rate, W/cm^2
R_a = afterbody radius, m
R_b = maximum probe radial dimension, m
R_c = corner radius, m
R_n = nose radius, m
Re_∞ = Reynolds number
s = distance along body surface measured from stagnation point, m
T = temperature, K
V = freestream velocity, m/s
X_i = mole fraction of species i
x = axial distance from stagnation point measured along symmetry axis, m
x_{cp} = center of pressure location, m
y = radial distance from symmetry axis, m
α = angle of attack, deg
γ = ratio of specific heats
λ = mean free path, m
ρ = density, kg/m^3

Subscripts

cg = center of gravity
cp = center of pressure
HS = hard sphere
w = surface values
∞ = freestream values

Received Jan. 20, 1998; revision received Aug. 15, 1998; accepted for publication Feb. 22, 1999.

*Aerospace Engineer, Aerothermodynamics Branch, Aero and Gas Dynamics Division. Fellow AIAA.
†Aerospace Engineer, Aerothermodynamics Branch, Aero and Gas Dynamics Division. Senior Member AIAA.
‡Aerospace Engineer, Aerothermodynamics Branch, Aero and Gas Dynamics Division.

Introduction

DURING the next decade, mapping and inspection missions to Mars will occur with considerable frequency by using orbiters, landers, penetrators, and sample return missions to prepare for possible human expeditions. The NASA Mars Exploration Program includes plans[1] for a pair of spacecraft to be sent to Mars every 26 months (on average). The missions launched between 1996 and 2001 will include a lander and an orbiter at each launch opportunity. This activity was initiated in late 1996 with two successful launches: first, the Mars Global Surveyor spacecraft, which provides an orbiting platform, and second, the Mars Pathfinder, which successfully executed entry, descent, and landing July 4, 1997.

The present study addresses the rarefied aerodynamics of two Mars Microprobes, penetrators that are enclosed in basketball-size aeroshells for thermal protection and stabilization during entry. As demonstrated in the present paper, rarefied aerodynamics can be a significant issue for entry capsules, particularly those without an active control system, as is the case for the Mars Pathfinder,[2,3] for the Stardust Sample Return Capsule,[4,5] and for the Mars Microprobes.[3,6] Because rarefied aerodynamic databases are required for design, operations, and postflight analyses, results of numerical simulations are presented. The simulations are achieved with the direct simulation Monte Carlo (DSMC) method of Bird.[7] DSMC results obtained by using both axisymmetric and three-dimensional solvers are presented and complemented with free-molecular and Newtonian results.

Upon arrival at Mars, the Microprobes will be released from the cruise-stage vehicle shortly after deployment of the Mars Surveyor 1998 Lander. Both Microprobes will then begin a free fall to the Mars surface. The capsule forebody is a spherically blunted 45-deg half-angle cone, followed by a hemispherical backshield with a maximum body diameter of 0.35 m. A unique aspect of the Microprobe entries is that the vehicles will encounter Mars' outer atmosphere in a random state, potentially tumbling after deployment from their host Mars 1998 Lander cruise-stage vehicle. The Microprobes depend on transitional flow aerodynamics to achieve an orientation that will not allow the afterbody thermal protection system to be compromised by heating at or near continuum flow conditions. Therefore, aerodynamic data for zero-to-large angles of incidence are provided for selected degrees of rarefaction. A discussion of the rationale for selecting the Mars Microprobes' aeroshell shape is given in Ref. 6, along with a description of its current aerodynamic database, which includes hypersonic rarefied, hypersonic continuum, supersonic, and transonic flow regimes.

Table 1 Freestream[a] and surface conditions for Mars Microprobe[b] overshoot trajectory

Altitude, km	V_∞, m/s	ρ_∞, kg/m^3	T_∞, K	T_w,[c] K	Kn_∞	$Kn_{\infty,\mathrm{HS}}$	Re_∞
126.72	6,909	2.6891×10^{-9}	171.4	300	50.5365	79.8036	1
113.20	6,916	2.3065×10^{-8}	154.5	400	5.7077	9.3040	7
98.69	6,922	2.3169×10^{-7}	136.3	500	0.5468	0.9262	75
91.41	6,923	7.6309×10^{-7}	124.6	600	0.1615	0.2812	266
80.47	6,913	3.8356×10^{-6}	133.8	900	0.0328	0.0560	1,261
73.42	6,884	9.4629×10^{-6}	146.4	1,200	0.0137	0.0268	2,879
64.29	6,751	3.4315×10^{-5}	143.1	1,500	0.0038	0.0063	10,430
54.88	6,168	1.2709×10^{-4}	149.9	1,800	0.0010	0.0017	34,000

[a]Freestream mole fractions are $X_{CO_2} = 0.95366$ and $X_{N_2} = 0.04634$, molecular weight = 43.2685, and diffuse surface with full thermal accommodation.
[b]Probe diameter = 0.325 m, $R_n = 0.08125$ m, and $R_c = 0.008125$ m.
[c]Assumed wall temperature values.

Computational Methods and Physical Models

The computational tools consisted of two DSMC codes complemented with a free-molecular/Newtonian code. The G2 code of Bird,[8] a two-dimensional/axisymmetric code, was used to provide zero-incidence DSMC calculations. G2 uses a body-fitted grid and has an extensive history of application and validation. For a G2 simulation, the computational domain can be subdivided into an arbitrary number of unstructured regions, with each region further subdivided into structured but variable size cells, and with the cells subdivided into subcells to promote nearest neighbor collisions.

The three-dimensional DSMC calculations were made using the DSMC analysis code (DAC) of LeBeau (described in Ref. 9). DAC uses a variable-resolution Cartesian grid currently consisting of two levels of cells. The resolution of the first level of cells is constant and is typically set based on the minimum desired flowfield resolution for a given problem. To further refine the flowfield grid in areas of increased density or high gradients, each level-1 cell can have an additional level of embedded Cartesian refinement. This second level of refinement is independent for each level-1 cell. The ability to refine the flowfield grid locally enhances DAC's ability to meet the spatial resolution required without excessive global refinement. The surface geometry for DAC is specified as a collection of planar triangular elements, which form an unstructured triangular grid. The surface grid is defined independently of the volume grid. The reduced volumes of Cartesian cells that are clipped by the surface are computed, and to minimize the computational effort required to determine molecule–surface interactions, the surface triangles are mapped to the Cartesian cells. Uncoupling the surface and volume grids is a desirable feature when calculating aerodynamic moments, particularly for highly rarefied flows in that the surface discretization can be resolved sufficiently to achieve accurate moment calculations without unnecessary flowfield resolution. More details concerning DAC features and capabilities are included in Ref. 9.

Free-molecular and Newtonian values presented herein were calculated by using the DACFREE code. This code was written by the second author's use of free-molecular[7] and modified Newtonian[10] analytical expressions. An unstructured triangular surface grid is used to define the surface geometry; it is the same grid used to define the surface geometry in DAC.

For both DSMC codes, the physical models are common. Molecular collisions are simulated by using the variable hard sphere (VHS)[7] molecular model. Energy exchange between kinetic and internal modes is controlled by the Borgnakke–Larsen[11] statistical model. A rotational relaxation collision number of 5 and a vibrational collision number of 50 were used. Solutions were obtained with and without chemical reactions for a constant freestream gas composition consisting of 95.4% CO_2 and 4.6% N_2 by volume. Parameters used to define the VHS model were a reference temperature of 3000 K and a viscosity temperature exponent of 0.8066.

For the calculations made with a reacting chemistry model, an updated version of the reaction set (54 reactions) used in the study by Hash and Hassan[12] was employed. This model consisted of eight species (O_2, N_2, O, N, NO, C, CO, and CO_2), while accounting for dissociation (40) and exchange (14) reactions.

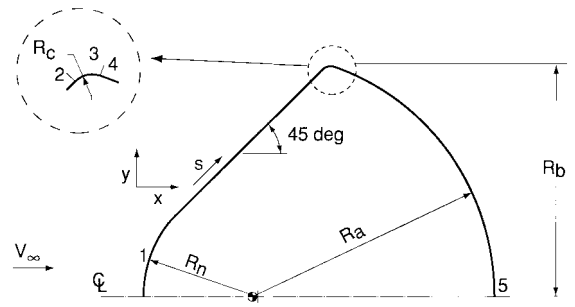

Location	x	y	s
1	0.02563	0.061872	0.06872
2	0.13619	0.17244	0.22509
3	0.14238	0.17500	0.23196
4	0.14528	0.17450	0.23492
5	0.26890	0.00000	0.46294
cg	0.08390	0.00000	—

Dimensions in m

Fig. 1 Mars Microprobe configuration: $R_n = 0.0875$, $R_c = 0.00875$ m, $R_a = 0.185$, and $R_b = 0.175$.

The surface boundary conditions assumed the gas–surface interaction to be diffuse with full thermal accommodation to a specified surface temperature. For those calculations with reacting chemistry, the surface was assumed to be noncatalytic.

Results and Discussion

Details of the hypersonic rarefied aerodynamics, as calculated with DSMC analysis for the Mars Microprobes, follows. Both reacting and nonreacting calculations with active internal energy modes have been made. While performing the computations, the baseline size of the Microprobe aeroshell was increased from an overall diameter of 0.325–0.350 m. The axisymmetric calculations were made for the small configuration (see Table 1 for various dimensions), whereas the three-dimensional simulations were made for the current baseline configuration shown in Fig. 1. The Microprobe geometry consists of a 45-deg half-angle spherically blunted forebody in which the nose radius is equal to half the base radius. The transition from forebody to afterbody is accomplished by means of an outer corner radius equal to 5% of the base radius ($R_b = 0.175$ m). The afterbody is hemispherical in shape, with the afterbody radius, $R_a = 0.185$ m, centered at the center of gravity located 0.0839 m aft of the forebody stagnation point. A discussion of the mission requirements and constraints leading to this particular geometry is given in Ref. 6.

Because the Microprobes will encounter the transitional flow region in a potentially tumbling mode, the manner in which they reorient themselves in a forward attitude and achieve a relatively small angle of attack will have important implications on the thermal protection system requirements.[13] Orientation is an important issue for the small Microprobe capsules because heating rates will be quite high. Furthermore, rarefied effects will persist to peak heating-rate conditions. Peak heating will occur near the lower altitude condition

Table 2 Mars Microprobe aerodynamic and heating results for overshoot trajectory and zero incidence

Altitude, km	$C_{D,P}$		C_D		Stagnation point q, W/cm^2	
	N.R.[a]	Reacting[b]	N.R.	Reacting	N.R.	Reacting
126.72	1.109	——	2.053	——	0.04	——
113.20	1.107	——	2.010	——	0.37	——
98.69	1.105	——	1.868	——	3.58	——
91.41	1.125	1.121	1.771	1.770	11.0	10.7
80.47	1.105	1.099	1.522	1.520	44.2	42.8
73.42	1.060	1.056	1.352	1.344	85.5	77.9
64.29	1.024	1.026	1.190	1.174	177.1	123.9
54.88	1.023	1.022	1.097	1.087	216.3	110.17

[a]Nonreacting flow results. [b]Reacting flow results.

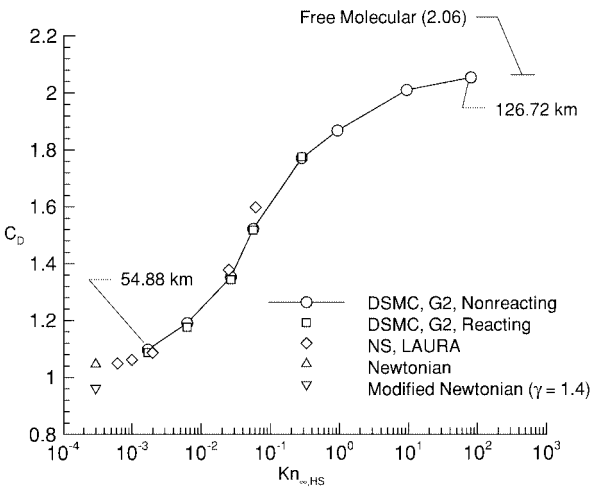

Fig. 2 Mars Microprobe drag coefficient for $\alpha = 0$ deg.

listed in Table 1, where the freestream conditions are for an overshoot trajectory (inertial entry angle of −12.58 deg), which produces the maximum integrated heat load condition.

Drag results from the axisymmetric G2 simulations both with and without reacting chemistry are included in Table 2 and are shown in Fig. 2. As expected, the change in the drag coefficient from continuum to free-molecular conditions is much larger for the more slender Microprobe than for the 70-deg half-angle spherically blunted cones such as Pathfinder[2]: 86% for Microprobe vs 24% for Pathfinder. Also, the contribution of friction to the total drag is significant: 7.4% at $Kn_{\infty,\mathrm{HS}} = 0.0017$ and 46% at $Kn_{\infty,\mathrm{HS}} = 80$. As was the case for Pathfinder,[3] the drag at zero incidence is insensitive to whether the calculations are made with or without a reacting chemistry model, provided the internal energy modes are active for both calculations. When the present results are compared (Fig. 2) with the Navier–Stokes (NS) calculations of Mitcheltree et al.,[6] agreement is good for Knudsen numbers on the order of 0.001. The NS results become questionable for Knudsen numbers larger than 0.05. The NS drag results are bracketed by Newtonian and modified Newtonian values.

Free-molecular results obtained with DACFREE are presented in Fig. 3. These calculations were made for freestream conditions corresponding to an altitude of 141.8 km (Table 3) and a wall temperature of 300 K. Unlike Pathfinder, Microprobe is statically stable at free-molecular conditions for $\alpha = 0$ deg and unstable for a backward attitude, a condition for which it was specifically designed, as discussed by Mitcheltree et al.[6] In fact, the restoring-moment coefficient decreases (Fig. 4b) as the probes descend into the continuum flow regime. The reduction in restoring moment is insignificant for angles of attack less than 25 deg but very significant for larger angles of attack.

Results of the transitional aerodynamics calculated with DAC are listed in Table 4 for various angles of attack and three levels of rarefaction. The freestream conditions (Table 3) are for a nominal entry trajectory corresponding to an inertial entry angle of −13.25

Table 3 Flight conditions[a] for Mars Microprobe[b] nominal trajectory

Altitude, km	V_∞, m/s	ρ_∞, kg/m^3	T_∞, K	T_w,[c] K	$Kn_{\infty,\mathrm{HS}}$
141.80	6,902	2.4438×10^{-10}	190.2	300	8.78×10^{2}
126.69	6,909	2.1000×10^{-9}	171.3	300	7.95×10^{1}
100.61	6,921	1.7066×10^{-7}	138.7	500	1.26×10^{0}
80.28	6,908	3.9287×10^{-6}	134.3	900	5.46×10^{-2}
53.84	6,090	1.4105×10^{-4}	154.5	2,000	1.52×10^{-3}

[a]Freestream mole fractions are $X_{CO_2} = 0.95366$ and $X_{N_2} = 0.04634$, molecular weight = 43.2685, and diffuse surface with full thermal accommodation.
[b]Probe diameter = 0.350 m, $R_n = 0.0875$ m, and $R_c = 0.00875$ m.
[c]Assumed wall temperature values.

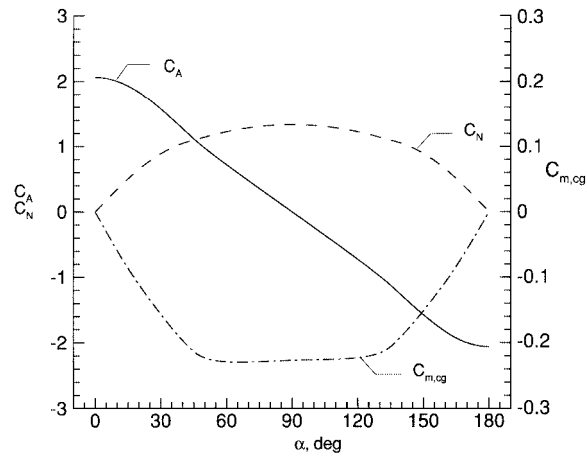

Fig. 3 Microprobe free-molecular aerodynamics.

deg at a radius of 3522.2 km. The angle-of-attack ranges were selected to capture approximately 99% of the envelope of possible total angles of attack based on six-degree-of-freedom Monte Carlo trajectory simulations. Figure 4 shows the variation of C_A, C_N, $C_{m,\mathrm{cg}}$, x_{cp}, C_L, C_D, and L/D for three levels of rarefaction as a function of angle of attack. The trends in the aerodynamic quantities with α (presented in Fig. 4) are consistent with the free-molecular and modified Newtonian data listed in Table 4. Mitcheltree et al.[6] discuss the use of bridging functions to achieve good agreement with the present Microprobe results.

The calculated heating rates are very dependent on the thermochemical state of the shock layer. Stagnation-point heating results with and without reacting chemistry models for a noncatalytic wall are presented in Fig. 5. The chemically reacting results reported by Moss et al.[3] for these conditions contained errors in the chemistry model. In the present study, the calculations have been repeated with the chemistry model corrected, and the calculations show a negligible effect on aerodynamics and less than a 10% effect on stagnation heating. The reduction in surface heating due to shock layer nonequilibrium chemistry, compared to nonreacting conditions, is about 3% at the 91.4-km altitude condition, but the reduction increases to about 51% at the 54.9-km condition (Table 2). With the current reacting chemistry modeling and the assumption of a noncatalytic surface, peak heating occurs between an altitude of 64 and 55 km, which is at a higher altitude than peak heating for the nonreacting calculations. Forebody surface heating-rate distributions for the four lowest altitude conditions of Table 2 are shown in Fig. 6. Heating along the conical forebody is about half the stagnation-point value. However, the heating-rate distributions along the conical forebody are shown to be dependent on rarefaction. This dependence on rarefaction is most apparent for the 54.9-km case in which heating along the conical forebody increases, rather than continually decreasing with distance s along the surface.

Trends evident in the heating-rate distributions are also manifested in the corresponding surface pressure distributions presented in Fig. 7. The surface pressure has been normalized by the freestream dynamic pressure. The increase in the pressure coefficient on the spherical nose section (with increasing rarefaction) is qualitatively correct. On the conical frustrum, the pressure coefficient distribution

Table 4 Mars Microprobe aerodynamics for nominal trajectory

Angle of attack, deg	C_A	C_N	$C_{m,0}$
	Altitude = 141.80 km	*Free molecular*	
0	2.061	0	0
5	2.046	0.176	−0.0721
15	1.928	0.508	−0.2081
30	1.574	0.893	−0.3703
45	1.120	1.100	−0.4769
60	0.724	1.229	−0.5235
75	0.360	1.311	−0.5429
90	0.001	1.338	−0.5472
105	−0.358	1.310	−0.5394
120	−0.725	1.227	−0.5169
135	−1.123	1.098	−0.4692
150	−1.574	0.894	−0.3654
165	−1.928	0.509	−0.2056
180	−2.061	0	0
	Altitude = 126.69 km	*DAC*	
0	2.054	0	0.0001
5	2.040	0.176	−0.0718
15	1.921	0.505	−0.2061
30	1.574	0.891	−0.3700
45	1.118	1.097	−0.4755
60	0.723	1.225	−0.5593
75	0.360	1.306	−0.5413
90	0.001	1.336	−0.5469
105	−0.358	1.305	−0.5370
120	−0.725	1.224	−0.5152
135	−1.122	1.095	−0.4672
150	−1.570	0.890	−0.3626
165	−1.921	0.506	−0.2040
180	−2.054	0	0.0002
	Altitude = 100.61 km	*DAC*	
0	1.901	0	−0.0004
5	1.891	0.156	−0.0657
15	1.788	0.452	−0.1910
30	1.470	0.794	−0.3403
45	1.071	0.991	−0.4391
60	0.716	1.126	−0.4911
75	0.369	1.222	−0.5161
90	0.001	1.252	−0.5138
	Altitude = 80.28 km	*DAC*	
0	1.536	0.001	−0.0013
5	1.520	0.128	−0.0580
15	1.424	0.360	−0.1650
30	1.180	0.607	−0.2838
45	0.904	0.734	−0.3525
60	0.656	0.846	−0.4035
	Altitude = 53.84 km	*Modified Newtonian ($\gamma = 1.4$)*	
0	0.962	0	0
5	0.958	0.076	−0.0450
15	0.926	0.219	−0.1298
30	0.830	0.382	−0.2260
45	0.690	0.461	−0.2668
60	0.511	0.472	−0.2564
75	0.279	0.460	−0.2215
90	0.013	0.449	−0.1787
105	−0.259	0.447	−0.1414
120	−0.504	0.449	−0.1177
135	−0.703	0.436	−0.1065
150	−0.862	0.360	−0.0872
165	−0.973	0.206	−0.0497
180	−0.101	0	0

is also seen to be influenced by rarefaction. For the smallest Knudsen number considered, there is a substantial overexpansion, followed by recompression, that influences the entire conical forebody, a qualitative behavior expected for this vehicle in hypersonic continuum flow. The expansion process diminishes with increasing rarefaction. This behavior is identical to that observed in the calculations by Moss et al.[14] for the Galileo Probe, also an entry capsule with a 45-deg spherically blunted forebody.

The extent to which the surface is catalytic to the recombination of atomic oxygen and carbon monoxide will also influence

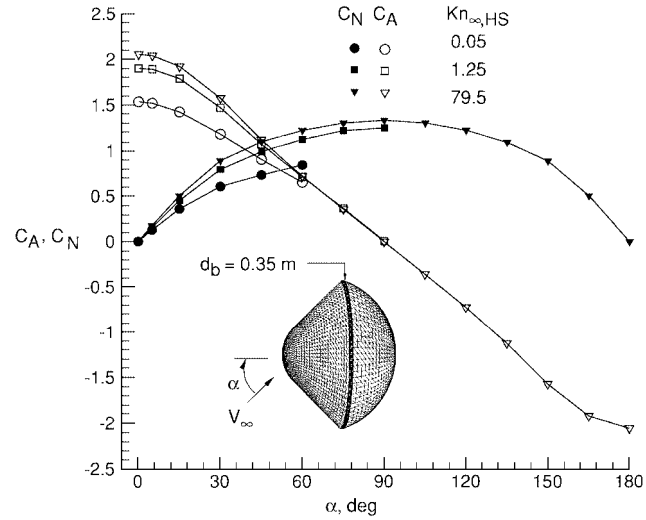

a) Axial and normal force coefficients

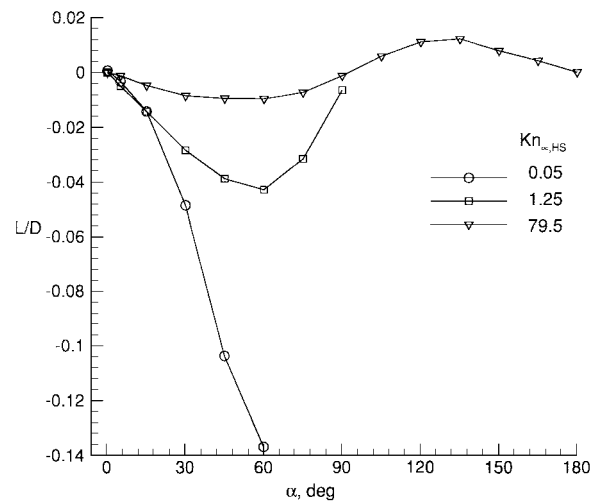

b) Lift-to-drag ratio

Fig. 4 Microprobe aerodynamics as a function of rarefaction and α.

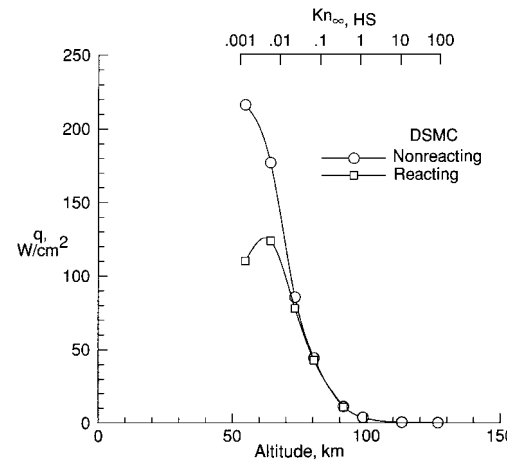

Fig. 5 Effect of nonequilibrium chemistry on stagnation-point heating for Microprobe.

the heating because the concentration of these species adjacent to the surface is significant (Fig. 8) near peak heating conditions. The depletion of CO_2, along the stagnation streamline (Fig. 9), is significant within the transitional flow regime, but not complete as would be the case for a larger capsule such as Pathfinder.[3] The smaller CO_2 depletion occurs because the shock layer thickness is about an order of magnitude smaller than that for Pathfinder at comparable altitudes.

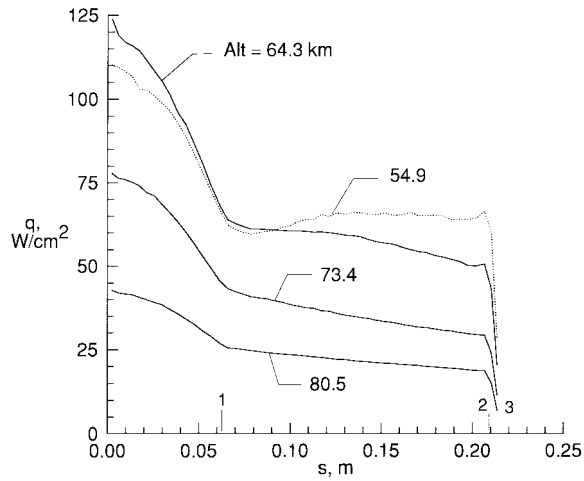

Fig. 6 Microprobe heating rate distributions.

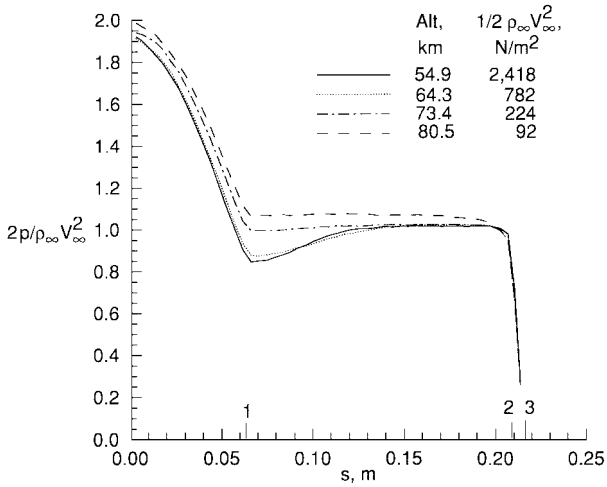

Fig. 7 Microprobe surface pressure distributions.

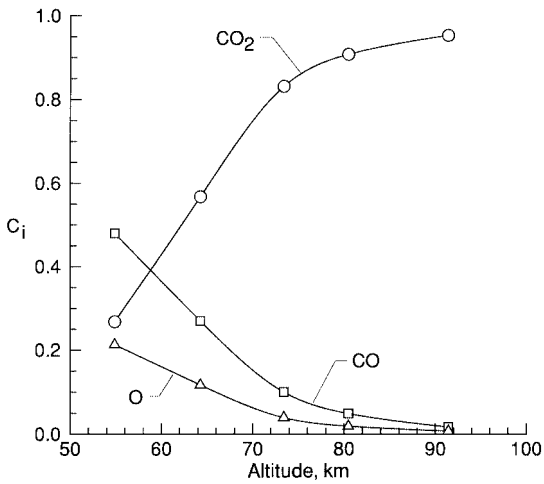

Fig. 8 Mass fraction of dominant species adjacent to forebody stagnation point.

The observed increase in CO_2 concentrations adjacent to a noncatalytic surface (Fig. 9) can potentially be attributed to two effects. One is the chemical exchange reactions; recombination is not a possibility because those reactions were omitted in the current chemistry model. The other possible contribution is that of thermal diffusion. Bird[15] has shown that thermal diffusion for similar hypersonic flows gives rise to an increase in heavy gas concentrations adjacent to surfaces. For large mass differences, thermal diffusion acts to concentrate the heavy gas in the cooler regions of the flow.

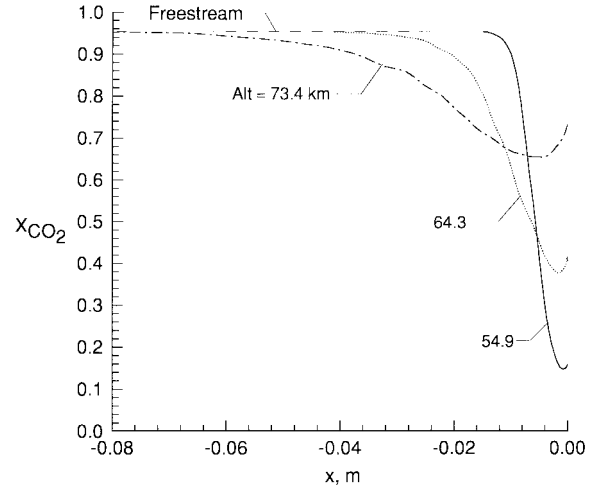

Fig. 9 CO_2 mole fraction profiles along stagnation streamline for Microprobe.

Conclusion

DSMC calculations complemented with free-molecular and Newtonian solutions have been made for the Mars Microprobe capsules. The numerical simulations encompass representative direct entry conditions from free-molecular to continuum hypersonic flows. Emphasis of the present study is the generation of transitional flow aerodynamic databases for preflight and postflight analyses. For the Mars Microprobes, the database has been used to validate bridging relations for aerodynamic coefficients, which in turn are used in trajectory simulations to establish that a vehicle is flyable. Computations for the Microprobes at zero incidence, using an eight-species chemistry model, provide information concerning heating and flowfield features.

Results of the computations show 1) excellent agreement between the axisymmetric and three-dimensional DSMC solutions for zero incidence, 2) excellent agreement between Navier Stokes and DSMC drag results for Knudsen numbers on the order of 0.001, 3) that the aerodynamic drag for the current blunt-body configurations at zero incidence is not influenced significantly by chemical reactions but is moderately sensitive to the vibrational modeling, and 4) a strong dependence of the flowfield structure and surface heating on the thermochemical state of the shock layer. With a significant degree of chemical nonequilibrium existing in the shock layer, assumptions concerning the thermal protection material catalytic activity will have a significant impact on both the predicted maximum heating rate and the total head load.

References

[1] Shirley, D. L., and McCleese, D. J., "Mars Exploration Program Strategy: 1995–2020," AIAA Paper 96-0333, Jan. 1996.

[2] Moss, J. N., Blanchard, R. C., Wilmoth, R. G., and Braun, R. D., "Mars Pathfinder Rarefied Aerodynamics: Computations and Measurements," *Journal of Spacecraft and Rockets*, Vol. 36, No. 3, 1999, pp. 330–339; also AIAA Paper 98-0298, Jan. 1998.

[3] Moss, J. N., Wilmoth, R. G., and Price, J. M., "DSMC Simulations of Blunt Body Flows for Mars Entries: Mars Pathfinder and Mars Microprobe Capsules," AIAA Paper 97-2508, June 1997.

[4] Wilmoth, R. G., Mitcheltree, R. A., and Moss, J. N., "Low-Density Aerodynamics of the Stardust Sample Return Capsule," *Journal of Spacecraft and Rockets*, Vol. 36, No. 3, 1999, pp. 436–441; also AIAA Paper 97-2510, June 1997.

[5] Desai, P. N., Mitcheltree, R. A., and Cheatwood, F. M., "Entry Dispersion Analysis for the Stardust Comet Sample Return Capsule," AIAA Paper 97-3012, Aug. 1997.

[6] Mitcheltree, R. A., Moss, J. N., Cheatwood, F. M., Greene, F. A., and Braun, R. D., "Aerodynamics of the Mars Microprobe Entry Vehicles," *Journal of Spacecraft and Rockets*, Vol. 36, No. 3, 1999, pp. 392–398; also AIAA Paper 97-3658, Aug. 1997.

[7] Bird, G. A., *Molecular Gas Dynamics and the Direct Simulation of Gas Flows*, Clarendon, Oxford, England, UK, 1994.

[8] Bird, G. A., "The G2/A3 Program Users Manual," G. A. B. Consulting, Pty, Killara, Australia, March 1992.

[9]Wilmoth, R. G., LeBeau, G. J., and Carlson, A. B., "DSMC Grid Methodologies for Computing Low-Density Hypersonic Flows About Reusable Launch Vehicles," AIAA Paper 96-1812, June 1996.

[10]Anderson, J. D., Jr., *Hypersonic and High Temperature Gas Dynamics*, McGraw–Hill, New York, 1989, pp. 53–56.

[11]Borgnakke, C., and Larsen, P. S., "Statistical Collision Model for Monte Carlo Simulation of Polyatomic Gas Mixture," *Journal of Computational Physics*, Vol. 18, No. 4, 1975, pp. 405–420.

[12]Hash, D. B., and Hassan, H. A., "Monte Carlo Simulation of Entry in the Martian Atmosphere," *Journal of Thermophysics and Heat Transfer*, Vol. 7, No. 2, 1993, pp. 228–232.

[13]Mitcheltree, R. A., DiFulvio, M., Horvath, T. J., and Braun, R. D., "Aerothermal Heating Predictions for Mars Microprobe," *Journal of Spacecraft and Rockets*, Vol. 36, No. 3, 1999, pp. 405–411; also AIAA Paper 98-0170, Jan. 1998.

[14]Moss, J. N., LeBeau, G. J., Blanchard, R. C., and Price, J. M., "Rarefaction Effects on Galileo Probe Aerodynamics," *Rarefied Gas Dynamics* 20, edited by C. Shen, Peking Univ. Press, Beijing, PRC, 1997, pp. 495–500.

[15]Bird, G. A., "Thermal and Pressure Diffusion Effects in High Altitude Flows," AIAA Paper 88-2732, June 1988.

R. D. Braun
Guest Editor